Maximizing Acceleration Capability of Magnetically Levitated Slice Motors

P. Karutz*, T. Nussbaumer**, W. Gruber*** and J.W. Kolar*

* ETH Zurich, Power Electronic Systems Laboratory, 8092 Zurich, Switzerland, karutz@lem.ee.ethz.ch
** Levitronix GmbH, Technoparkstrasse 1, 8005 Zurich, Switzerland
*** ACCM GmbH (Johannes Kepler Universität Linz), Altenbergerstr. 69, 4040 Linz, Austria

Abstract – Over the last few years industry branches with a growing demand for high purity and contamination-free high-acceleration spin processes, such as biotechnology, chemical, pharmaceutical and semiconductor industry, have tightened their cleanness specifications for the process environments. A recent trend to meet these specifications is to use magnetically levitated slice motors with air gaps being large enough to insert a process chamber wall, which assures the hermetical sealing of the process. The drive design of these motors is challenging due to the employed large air gaps and the demand for maximum acceleration capability. Separate design considerations for a non-saturating stator drive claw geometry and for an appropriate drive winding number have been proposed in the past, not considering the interdependencies of these two designs. This paper presents an overall optimization procedure yielding for minimal acceleration times of magnetically levitated slice motors for different speed ranges and verifies the considerations by measurements on a prototype system.

I. Introduction

Nowadays, a growing demand for high purity and contamination-free spin processes can be identified for biotechnology, chemical, pharmaceutical and semiconductor industry due to the rapidly increasing complexity and sensitivity of the process objects. Furthermore, process dependent conditions (process gas, gas pressure, temperature) have to be guaranteed for an optimal process result. These specifications can be ensured by encapsulating the revolving rotor by a hermetically sealed process chamber in combination with a contactless levitation method that can be provided by the use of active magnetic bearings (AMB). This type of bearing offers the advantage of almost unlimited life time, adjustable bearing parameters and wearless and lubrification-free operation, resulting in a high level of purity. For a big diameter-to-height ratio of the rotating device as it is the case for such applications, the technology of magnetically levitated slice motors [1]-[5] can be employed advantageously. These setups ensure a high level of compactness, which saves valuable space within the process equipment.

Considering the process specifications and the application areas of interest, three main motor requirements can be stated. First, the process dependent maximum rotation speed has to be reached. Secondly, the acceleration times between the process speeds have to be minimal in order to reduce the equipment's operating costs, consequently demanding for a high torque capability. And last, the construction of a mechanically robust and chemically resistant chamber wall typically requires a large air gap. In Fig. 1 a common drive concept used for the

applications at hand is depicted, illustrating a drive claw (forming a part of a drive phase) with concentrated windings, the process chamber wall and the interior of the rotor (with its permanent magnets and an iron ring providing the flux feedback path). Concentrated windings are usually utilized when the circumferential space has to be used efficiently while ensuring a low profile height, since they can be fitted into the gaps between the bearing claws, which ensure the levitation of the rotor [4].

The need for high torque up to high rotation speeds along with the large air gap asks for a high drive current in the concentrated windings, wherefore an appropriate design of the drive lamination stack is crucial for high acceleration drives. In [6] it has been shown that saturation effects reduce the effective torque and therefore increase the acceleration time t_{acc}. The authors proposed to implement simple L-shaped drive claws instead of conventional claws with expanded pole shoe tips [7], whereby saturation effects can be avoided effectively. However, saturation may still appear in L-shapes for certain drive claw dimensions together with certain levels of ampere-turns and degrade the effective torque, as will be shown in this paper.

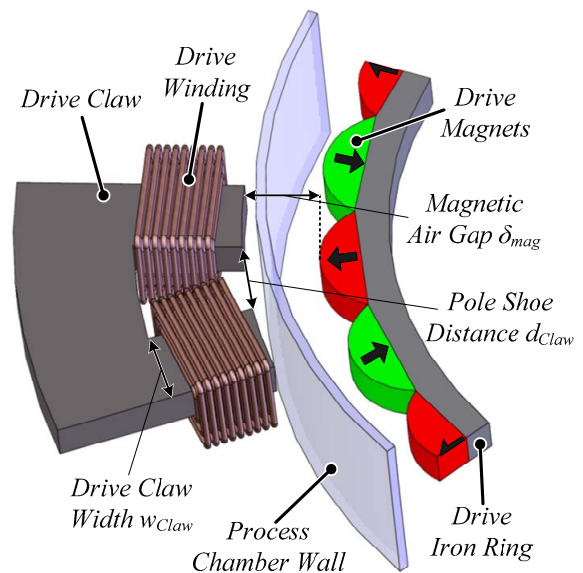Another aspect is the limitation of the torque for higher rota-

Fig. 1: Schematic cut view showing the arrangement of the concentrated windings, the air gap intersected by the process chamber wall and the rotor in the inside of the chamber.

1

tional speeds by the drive coil inductance. Based on this fact, an optimal number of drive windings can been found for a certain speed range, as it has been done in [4]. However, the negligence of the before-mentioned dependency on the drive claw geometries with the associated saturation aspects may lead to a non-optimal or even erroneous design.

Therefore, in this paper an optimization procedure is developed that allows the optimal selection of the drive claw dimensions and the winding number in dependency on the speed range based on the general physical dependencies of the machine and on 3D-FEM simulations.

The limited circumferential space available in a magnetically levitated slice motor results in limited degrees of freedom during the drive claw design. A magnetically levitated 2-level motor, which was introduced in [3], is used in the following as an exemplary motor concept to visualize this issue and to prove the optimization results. This motor concept has the advantage of decoupled iron paths for the bearing force and motor torque generation, which allows an isolated view on the mechanisms in the stator claws. However, the optimization steps can be directly adapted for the motor in [4] and with the considerations of the influence of the bearing also for [1], [2] and [5].

The setup and the basic functionality of the magnetically levitated slice motor are introduced in section II. Subsequently, in section III the acceleration behavior and the resulting optimization parameters are described. The optimization procedure and its results are presented in section IV, whereby the experimental verification of the results is presented in section V.

II. EXEMPLARY MOTOR CONCEPT

The main components of the magnetically levitated 2-level motor [3] are depicted in the schematic top and side view in Fig. 2. This motor combines a two phase homopolar magnetic bearing and a two phase permanent magnet synchronous drive on two axially and circumferentially shifted height levels.

The bearing forces are generated contactless through the process chamber wall on the upper level of the motor. The axial displacement and the tilting of the rotor are passively stabilized by reluctance forces [1]. Since these axial stabilizing forces cause a destabilizing radial force [8], the radial displacement has to be controlled actively. With the aid of the bearing windings the air gap flux can be weakened or amplified, resulting in a rotor movement into the direction of the higher flux density. Both of the two bearing phases consist of two opposing bearing claws. In order to compensate all radial deflections of the rotor the bearing phases are arranged perpendicularly to each other. Due to the low height compared to the diameter this motor needs bearing units only at one axial level, which results in a very compact setup. However, in order to generate the necessary bearing forces a minimum circumferential space for the bearing units have to be ensured. This directly limits the available circumferential space for the drive claw, which is placed in between the bearing claws in order to keep the setup compact. For the sake of brevity a more detailed description of the magnetic bearing and the levitation mecha-
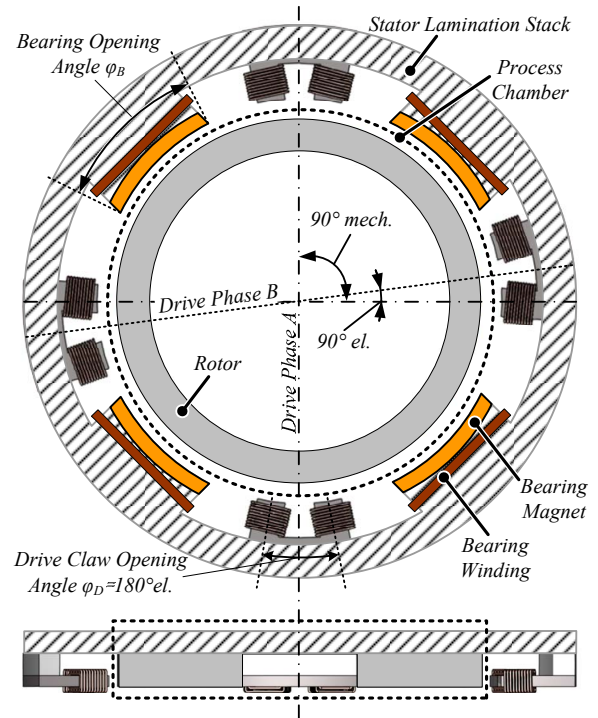

Fig. 2: Schematic top view and side view of the magnetically levitated 2-level motor showing the circumferential separation of the drive and bearing unit. Additionally, the angular offset of 90°mech. ± 90°el. of drive phase B with respect to drive phase A is indicated.

nisms is omitted, but the interested reader is referred to [3].

On the lower level of the motor the two-phase permanent magnet synchronous drive is situated. It consists of the drive claw including the drive windings and the permanent magnets located on the drive iron ring providing the flux feedback path (cf. Fig. 1). The permanent magnets are round-shaped and with alternating, diametrical magnetization in order to provide a sinusoidal-like flux density distribution in the air gap. The drive windings are fed with an appropriate current I_D that is kept in phase with the induced voltage U_{ind} through field oriented control. Each of the two drive phases consists of two opposing drive claws that are arranged in between the bearing claws. The drive claw has preferably an opening angle of $\varphi_D = 180°$el. as depicted in Fig. 2. This leads to a maximum achievable torque as stated already in [3]. Since the rotor drive magnets always attract the iron of the drive claw independently of their magnetization direction, there exist priority positions of the rotor. The drive claw opening angle φ_D in combination with the priority positions demands for an additional 90°el. phase shift (in addition to the 90°mech. phase shift) between the two drive phases, because otherwise the rotor would lock in one of the priority positions and no torque could be generated.

This also guarantees a constant motor torque independently of the rotor position. Since the product of the in-phase sinusoidal induced voltage and the sinusoidal drive current (due to the field oriented control) results in a square sinus torque in the first drive phase. The additional 90°el. phase shift of the second drive phase creates a square cosine torque. Consequently,

the sum of the single phase torques results in a constant torque independently of the rotor position.

$$\sin^2(\omega \cdot t) + \cos^2(\omega \cdot t) = 1, \qquad (1)$$

The acceleration behavior and the influence of constructional parameters are explained in more detail in the next section.

III. ACCELERATION BEHAVIOR

The acceleration time t_{acc} of the motor can be expressed by

$$t_{acc} = \frac{J}{k_{Uind}} \cdot \left(\frac{2\pi}{60}\right)^2 \cdot \int_0^{\Delta n_R} \frac{1}{I_{D(n_R)}} dn_R \qquad (2)$$

with the rotors moment of inertia J, the induced voltage factor k_{Uind}, the rotation speed n_R and the drive current I_D [4] . The induced voltage factor k_{Uind} is defined by the ratio of the induced voltage U_{ind} and the rotation speed

$$k_{Uind} = \frac{U_{ind}}{n_R}, \qquad (3)$$

which addresses the linear behavior of the induced voltage. The induced voltage U_{ind} can be described by

$$U_{ind} \sim \frac{d\Phi_{PM}(I_D, \varphi_{el})}{d\varphi_{el}} \qquad (4)$$

with the permanent magnet flux Φ_{PM} and the electrical rotation angle φ_{el}.

Judging from (2) and (3) the aim of acceleration time minimization can be achieved if both factors U_{ind} and I_D are maximized. The induced voltage U_{ind} can be generally maximized by three methods.

Firstly, the induced voltage is directly proportional to the drive winding number N_D, which should therefore be as large as possible in order to maximize U_{ind}.

Secondly, due to possibly occurring saturation effects the magnitude of the induced voltage is influenced by the drive current I_D. In [6] it was shown that the drive claw shape influences the affinity of the drive claws to go into saturation for certain levels of ampere-turn Θ, being defined as

$$\Theta = N_D \cdot I_D. \qquad (5)$$

Especially for motors with concentrated drive windings, high acceleration requirements and large air gaps the conventional expanded pole shoe tips cause paths of reduced magnetic resistance similar to a magnetic shortcut, consequently lowering the effective torque. Here, the authors come to the conclusion that these paths can be effectively avoided in whole operating range when the L-shaped drive claw shown in Fig. 1 is used, given that a certain minimum cross-sectional area is provided. Both the drive claw height h_{Claw} and the claw width w_{Claw} increase the cross section of the bearing claw. Since the increase of the claw height is not fulfilling the demand for a compact setup (as the rotor height would have to be increased, too) the claw width w_{Claw} is the only parameter to be optimized in order to guarantee a non-saturating drive claw within the whole operating range. It has to be considered that if w_{Claw} is increased beyond the optimal width, the distance between the two pole shoes d_{Claw} (cf. Fig. 1) may get smaller than the magnetic air gap δ_{mag}. This causes a situation similar to a magnetic shortcut, which decreases the effective torque. Concluding from the saturation point of view the induced voltage U_{ind} can be maximized for an optimal drive claw width and a minimal ampere-turns value Θ, directly leading to minimal drive current I_D and drive winding number N_D.

Thirdly, the induced voltage can be maximized, if the derivation of the permanent magnet flux Φ_{PM} with respect to the rotational angle φ_{el} is maximized. The flux linkage, which is the permanent magnet flux lines that are embraced by the drive windings, can be maximized by increasing the cross section of the drive claw facing the drive permanent magnets. Again, due to the compactness restrictions this is preferably done by increasing the claw width w_{Claw}.

For a maximum motor torque M_D also the drive current I_D has to be maximized. According to [4] the drive current amplitude $\hat{I}_D$ can be expressed as

$$\hat{I}_D = \frac{-\hat{U}_{ind} \cdot R_D \pm \sqrt{(R_D^2 + \omega^2 \cdot L_D^2) U_{DC}^2 - \omega^2 \cdot L_D^2 \cdot \hat{U}_{ind}^2}}{R_D^2 + \omega^2 \cdot L_D^2}, \qquad (6)$$

with the drive phase winding resistance R_D, the drive phase winding inductance L_D, the DC-link voltage U_{DC} of an inverter in full bridge configuration driving the bearing coil and with the electrical angular frequency ω. Basically, (6) addresses the current limiting effects of the induced voltage and the inductive voltage drop, which are both dependent on the rotation speed $n_R = 60 \cdot \omega /(2\pi p)$ with the pole pair number p. Additionally, the resistive voltage drop is included into (6) for the sake of completeness, but it has only a minor influence on the resulting drive current. Typical drive current characteristics in dependency of the rotation speed n_R are depicted in Fig. 3(a). For low rotation speeds n_R the drive current is limited to the maximum output current of the power electronics $I_{PE,max}$, since the influence of the induced voltage and inductive voltage drop is still low. The current starts to decrease at a certain rotation speed depending on the drive winding number. Therefore, in order to maximize the current, the induced voltage U_{ind} and the drive phase inductance L_D should be reduced.

However, according to (2), the acceleration time t_{acc} and consequently the torque depends on the reciprocal product of the drive current I_D as well as the induced voltage U_{ind}, which demands for an increase of U_{ind}. Hence, this opposing influence of U_{ind} demands for an optimization of the drive winding number in order to have a maximum torque. The dependence of the acceleration time t_{acc} on the drive winding number N_D for different rotation speeds n_R is depicted in Fig. 3(b). The fastest acceleration ($t_{acc} = 3.5$ s) towards a rotation speed of $n_R = 2000$ rpm can be accomplished by the employment of a drive winding number of $N_D = 600$. For lower rotation speeds smaller drive winding numbers would be more appropriate and the same applies inversely for higher rotation speeds. Hence, the minimization of the acceleration time as a measure for the drive torque has to be carried out also considering the rotation speed span Δn_R, since it is shifting the optimization point of the
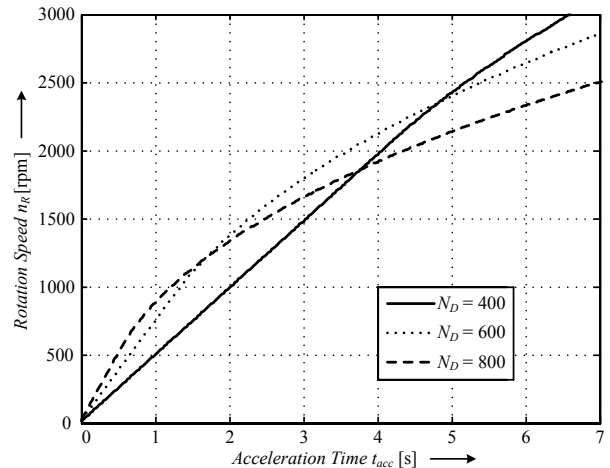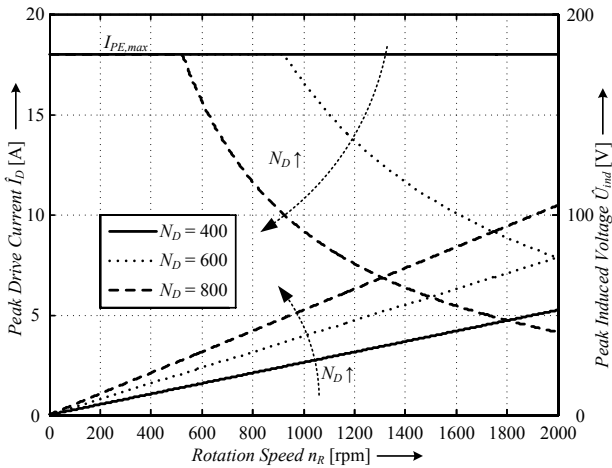
3

Fig. 3: (a) Achievable drive current $\hat{I}_D$ (for $I_{PE\,max}$ = 18 A) and induced voltage $\hat{U}_{ind}$ in dependency of the rotation speed n_R for different drive phase winding numbers N_D and (b) estimated acceleration performance of the exemplary motor.
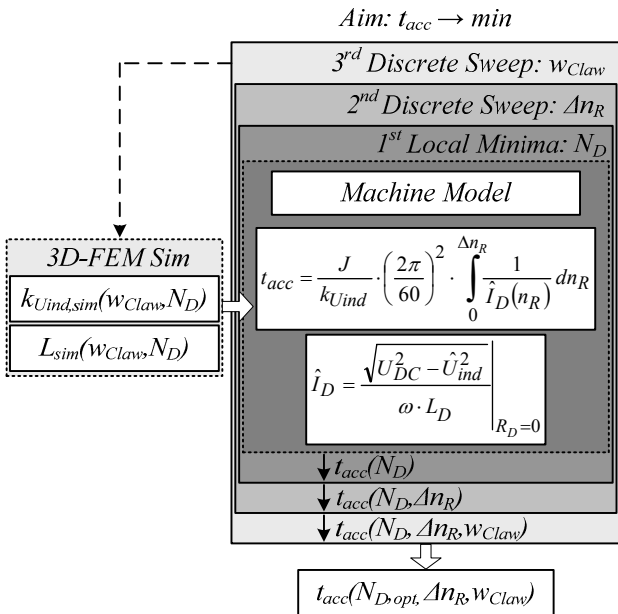

Fig. 4: Optimization procedure for maximum acceleration capability, showing three loops of parameter sweeping with 3D FEM simulation data being fed into the analytical machine model.

Fig. 5: Dependency of the acceleration time t_{acc} on the phase drive winding numer N_D presented for a constant drive claw width w_{claw} = 25 mm and different rotation speed spans Δn_R. The optimal winding number $N_{D,opt}$ is exemplarily indicated for an acceleration up to 2000 rpm.

design. In order to maximize the overall acceleration capability an optimization considering the drive claw width w_{Claw}, the drive winding number N_D and the rotation speed span Δn_R has to be carried out. A description of this optimization routine is given in the next section.

IV. OPTIMIZATION ROUTINE

A three-loop optimization procedure as depicted in Fig. 4 was developed in order to determine the optimal constructional parameters (drive claw width w_{Claw} and drive winding number N_D) for a minimal acceleration time t_{acc} within a certain rotation speed span Δn_R. Since the flux distribution in the air gap is highly non-linear, an analytical derivation of the induced voltage and the drive inductance is imprecise. Therefore, as depicted in Fig. 4 the optimization procedure is fed externally by
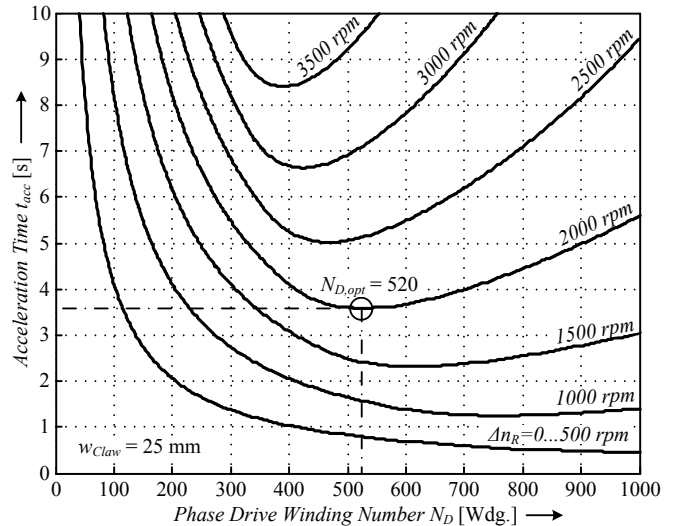
3D-FEM simulation results of the simulated induced voltage constant $k_{Uind,sim}$ and the effective drive inductance L_{sim} in dependency on N_D and w_{Claw}.

In the first loop the drive current dependency of (6) is used in the dynamic machine model in order to solve the integral giving the resulting acceleration time t_{acc}. Hereby, the drive claw width w_{Claw} and the rotation speed range Δn_R are left constant. The repetitive variation of the drive winding number N_D in a reasonable range results in a single curve of Fig. 5. Exemplarily, the optimal drive winding number $N_{D,opt}$ = 520 for a minimal acceleration time of t_{acc} = 3.5 s during an acceleration up to 2000 rpm and drive claw width of w_{Claw} = 25 mm can be determined from Fig. 5.

The second loop adds the variation of the rotation speed range Δn_R into the optimization procedure, which delivers the array of curves shown in Fig. 5. For each of the curves, there exists an optimal winding number $N_{D,opt}$. Here, the tendency towards
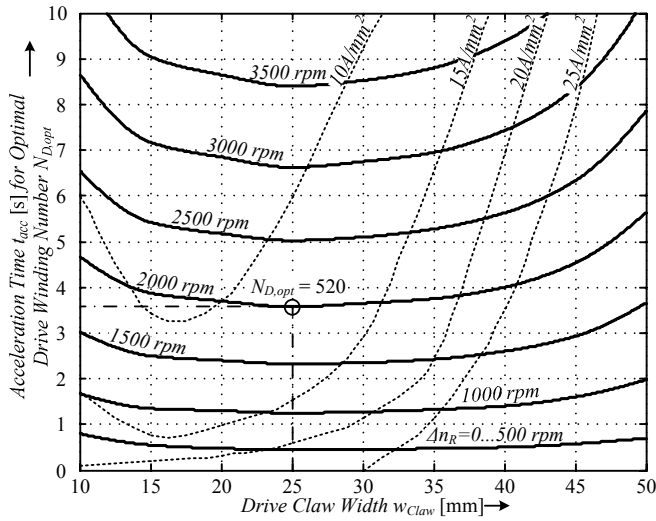
Fig. 6: Optimization result showing the acceleration time t_{acc} with the optimal winding turn number $N_{D,opt}$ in dependency of the stator claw width w_{Claw} and the rotation speed range Δn_R, while the dotted lines indicate areas of different occurring current densities within the drive winding wire.
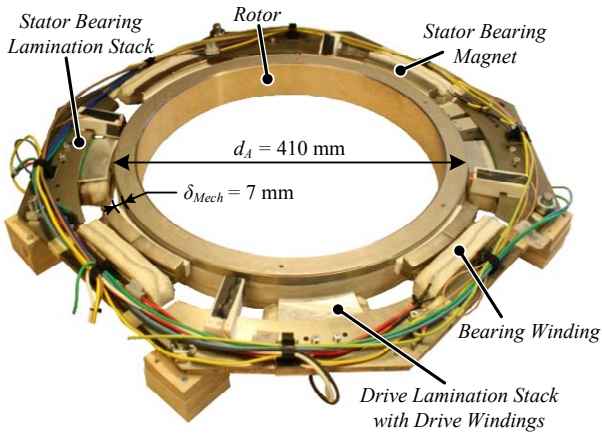

Fig. 7: The laboratory prototype used for the experimental verification measurements employs two drive phases. Each drive phase consists of two drive claws with $w_{Claw} = 25$ mm and each drive claw has two coils with the coil winding number $N_C = N_D/4 = 130$ windings.

lower N_D for higher Δn_R is already visible.

Finally, the variation of the drive claw width is implemented into the third loop. As a result, various curve arrays as in Fig. 5 are generated for different drive claw widths, where for each combination of Δn_R and w_{Claw} the optimal winding number can be determined. In Fig. 6 the resulting acceleration time for different drive claw widths is depicted, whereby each point is characterized by the optimal drive winding number $N_{D,opt}$. Generally, the drive claw with $w_{Claw} = 25$ mm shows the lowest acceleration times for the depicted speed ranges. Around this optimum the time difference is rather low, provided the corresponding optimal drive winding number is implemented. How ever, as stated before, the acceleration time rises rapidly for significantly smaller and larger values of w_{Claw}. This is due to the effect that small drive claw widths demand higher drive
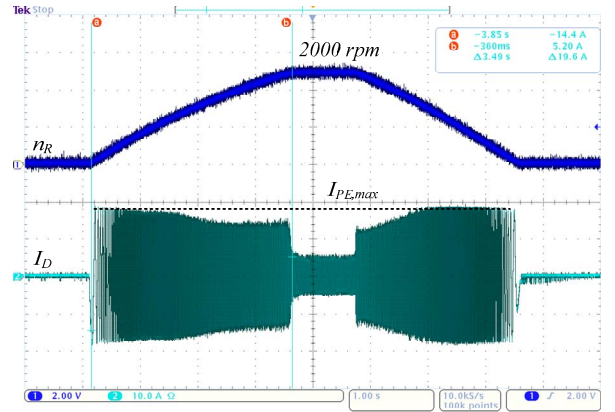

Fig. 8: Acceleration behavior of the laboratory prototype from 0 to 2000 rpm for a maximum current limited by the power electronics to $I_{PE,max} = 18$ A (with a drive coil winding number $N_C = N_D/4 = 130$, this results in a maximum ampere-ratio of $\Theta_{Peak} = 2 \cdot 2860$ A·turns) in 3.5 s and deceleration in 2.6 s (scales: 800 rpm/div., 10 A/div., 1 s/div.).

TABLE 1: DESIGN DATA OF THE EXPERIMENTAL SETUP

Outside rotor diameter d_A	410 mm
Mechanical air gap δ_{Mech}	7 mm
Number of pole pairs p	12
Specified Rotation Speed Span Δn_R	2000 rpm
Opt. Drive Winding Number $N_{D,opt}$	520
Acceleration Time t_{acc} for Δn_R	3.5 s
Rotor mass m	5 kg

winding numbers due to the reduced coil flux linkage and the occurring saturation effects. For larger values of w_{Claw} the magnetic resistance between the drive claws decreases, which augments the tendency for saturation of the drive claws and consequently lowers the effective torque. Additionally, the limited space between the pole shoes increases the current density in the wires of the drive winding, since for a given optimal drive winding number the diameter has to be reduced. In Fig. 6 this effect is addressed by the dotted lines defining different areas of current density. Hence, especially for the motor at hand and the targeted rotation speed span up to 2000 rpm drive claw widths larger than 30 mm seem inappropriate due to resulting high thermal stress of the drive windings.

From the results of the presented optimization procedure the drive claw width $w_{Claw} = 25$ mm with an optimal winding number $N_{D,opt} = 520$ was implemented in an experimental prototype. The next section presents the results of the experimental verification.

V. EXPERIMENTAL VERIFICATION

The laboratory prototype used for the experimental verification is depicted in Fig. 7 and the main parameters are summarized in Table 1. Due to the cost and work efforts involved with the manufacturing of a drive claw including the drive windings, only the optimal point for the specified rotation speed span of $\Delta n_R = 2000$ rpm is verified. Correspondingly, an

acceleration behavior of the motor is depicted in Fig. 8. Here, the rotation speed of $n_R = 2000$ rpm is reached within $t_{acc} = 3.5$ s. The comparison of this measurement with the optimal point depicted in Fig. 6 shows a very good accordance. This demonstrates that the method for the acceleration capability maximization is precise and applicable for the motors at hand.

VI. CONCLUSION

In this paper the maximization of the acceleration capability of magnetically levitated slice motors with large air gaps was investigated. An exemplary motor concept was used to show the acceleration capability limiting influence of the drive claw saturation and the inductive voltage drop over the drive winding especially for the use of concentrated windings. In the following, the drive claw width and the drive winding number were indentified as the constructional parameters that both have to be considered in order to reach an ultimately minimized acceleration time. For the maximization of the acceleration capability a three loop optimization routine considering these constructional parameters and that is fed externally by 3D finite element simulation results was described. The results

of the optimization were presented and the experimental verification on a laboratory prototype showed a good match of the optimization and the measurement.

REFERENCES

[1] R. Schoeb, N. Barletta, "Principle and Application of a Bearingless Slice Motor," JSME Int. Journal Series C, pp. 593-598, 1997.
[2] A. Chiba, D.T. Power, M.A Rahman, "Chracteristics of a Bearingless Induction Motor," IEEE Trans. Magnetics, vol. 27, no. 6, Nov. 1991.
[3] P. Karutz, T. Nussbaumer, W. Gruber, J.W.Kolar, "The Bearingless 2-Level Motor, " *Proc. of the 7th Int. Conf. on Power Electronics and Drive Systems*, Bangkok, Thailand, Dec. 2007
[4] T. Schneeberger, J. W. Kolar, "Novel Integrated Bear-ingless Hollow-Shaft Drive," Proc. of the IEEE Ind. Applic. Conf. IAS, Tampa (USA), 8 – 12 Oct. 2006.
[5] W. Gruber, W. Amrhein, "Design of a Bearingless Segment Motor," *Proc. of the 10th Int. Symp. on Magnetic Bearings* Martigny, 2006.
[6] P. Karutz, T. Nussbaumer, W. Gruber, J.W.Kolar, "Saturation Effects in High Acceleration Bearingless Slice Motors, "*Proc. of the 2008 IEEE International Symposium on Industrial Electronics,* Cambridge (UK), 2008
[7] H.-P. Nee, "Rotor slot design of inverter-fed induction motors," *Seventh International Conference on Electrical Machines and Drives*, no. 412, pp.52-56, 11-13 Sep 1995.
[8] J.-P. Yonnet, "Permanent magnet bearings and couplings," *IEEE Trans. Magnetics*, vol.17, no.1, pp.1169- 1173, Jan. 1981.